OAK RIDGE
NATIONAL LABORATORY
MANAGED BY UT-BATTELLE
FOR THE DEPARTMENT OF ENERGY

ORNL/LTR-2012/440

Light Water Reactor Sustainability

Cast Stainless Steel Aging Research Plan

September 2012

Prepared by:

T. S. Byun and J. T. Busby

Oak Ridge National Laboratory

UT-BATTELLE
ORNL-27 (4-00)

ORNL/LTR-2012/440

Light Water Reactor Sustainability

Cast Stainless Steel Aging Research Plan

T. S. Byun and J. T. Busby
Materials Science & Technology Division
Oak Ridge National Laboratory

Date Published: September 2012

Prepared under the direction of the
U.S. Department of Energy
Office of Nuclear Energy
Light Water Reactor Sustainability
Materials Aging and Degradation Pathway

Prepared by:
OAK RIDGE NATIONAL LABORATORY
Oak Ridge, Tennessee 37831-6283
managed by
UT-BATTELLE, LLC
for the
U. S. DEPARTMENT OF ENERGY
under contract DE-AC05-00OR22725

CONTENTS

Page

Cast Stainless Steel Aging Research Plan

T. S. Byun and J. T. Busby
Oak Ridge National Laboratory

ABSTRACT

This work plan proposes to build a systematic knowledge base for the thermal aging behavior of cast stainless steels (CASSs) within a limited time of five years. The final output of execution of the plan is expected to provide conclusive predictions for the integrity of the CASS components of LWR power plants during the extended service life up to and beyond 60 years. Mechanical and microstructural data obtained through accelerated aging experiment and computational simulation will be the key input for the prediction of CASS behaviors and for the integrity analyses for various CASS components. While the accelerated aging experiment and computational simulation results will comprise the main components of the knowledge base for CASS aging, the data obtained in-situ at power plants or from plant-served components are needed to validate the accelerated aging methodology as well as to provide realistic guidelines for plant life extension. In addition to using existing database, therefore, a systematic campaign to obtain mechanical data from used materials or components is pursued and a semi-nondestructive testing technology is developed or acquired if needed. Further, the detailed studies on aging and embrittlement mechanisms as well as on deformation and fracture mechanisms are performed to understand and predict the aging behavior over extended lifetime. The following sections include an introduction to CASS thermal aging, microstructural backgrounds, and a five year plan.

1. INTRODUCTION

The cast stainless steels (CASSs) are highly corrosion-resistant iron-chromium-nickel alloys with austenite single phase or austenite-ferrite duplex structure and have been used for a variety of applications in nuclear power plants. The CASSs are important materials in modern LWR facilities since a massive amount of the alloys is used for majority of pressure-boundary components in reactor coolant systems. Relatively few critical degradation modes of concerns are expected within the current designed lifetime of 40 years given that the CASS components have been processed properly [1-7]. On the integrity of CASS components beyond this timeframe, however, no conclusive prediction can be made because no direct experience with these materials exists. Further, the accelerated aging experiments, which have been performed in the past typically near or at 400 °C, were yet to be validated for simulation of lower temperature phenomena. The current status is therefore that, although the vast majority of the current and future nuclear power plants are expected to be operational for the extended lifetimes of 60 years or potentially longer, the behaviors of CASSs after such prolonged periods are largely unknown. An assessment of mechanicalï property degradation due to thermal embrittlement is required to evaluate the performance of cast stainless steel components during prolonged exposure to service temperatures, because a rupture of the primary pressure boundary could lead to a lossï ofï coolant accident and possible exposure of the public to radiation.

The CASSs are typically graded by their microstructure [8,9]. There are fully austenitic grades such as grade CN7 (with up to 30 wt% Ni) and martensitic grades with lower Cr and Ni contents (13 and 4 wt.%, respectively). A major class of CASS between these two groups is the duplex austenitic-ferritic alloys. These include the CF family of cast grades which have approximately 19% Cr and 9% Ni. Common composition limits for these alloys are shown in Table 1 along with comparative composition limits for wrought equivalent steels. In CASSs, the main chemical elements ultimately determine their microstructure. The nuclear grade CASSs, CF3 and CF3M, for example, can contain 3 to 30% ferrite in an austenite matrix, although CF3 alloys typically contain 10 to 20 percent ferrite. The CF8 alloys have only about 10 percent ferrite. The amount of ferrite varies strongly with composition and more ferrite content generally leads to higher tensile strength.

A variety of CASSs have been used in nuclear power plants, depending on reactor models and years built. Common alloys in service include the CF3 and CF8 series of alloys with the CF3, CF3A, CF3M, CF8, CF8A, and CF8M being the most prominent choices [3-9]. Typical nuclear power plant applications and material grades of CASS include the use of CF8A, CF8M, and CPF3M for reactor coolant and auxiliary system piping. Reactor coolant pump casings are typically made from grade CF8, CF8A, or CF8M CASS. Reactor coolant valve bodies and fittings often use CF8A or CF8M. In later construction applications and replacements CF3s have been used rather than CF8s. These alloys are exposed to elevated temperatures, internal pressures, and corrosive environments. Piping and pump casings in BWRôs may be exposed to normal and hydrogen water chemistries (NWC and HWC), and in some locations, to lower level irradiation. In PWRôs, these alloys experience the primary water environment.

Historically, the cast stainless steel grades have performed well in nuclear applications [1-7]. There have been limited cases of SCC in CASS components in both BWRôs and PWRôs; however, these are attributed to irregularities in composition or microstructure primarily caused by improper fabrication processes rather than general vulnerabilities [1,2]. In BWRôs, thereôs an

increased susceptibility to SCC in areas of cold-work or weldments. To date, there has been no record of IASCC in these components. Similarly, there are no concerns for CASS components related to general or localized corrosion, fatigue, flow-accelerated corrosion, or wear for current lifetimes.

Under extended service scenarios; however, there should be major degradation modes to consider. Thermal aging could lead to decomposition of phases, resulting in increased susceptibility to embrittlement, irradiation-induced degradation, SCC, and general corrosion. The details of these degradation modes and their mechanisms are reviewed and summarized in the following section. The main objective of this detailed review is to find out the material degradation modes that may generate structural risks during an extended operation for Ó60 yrs, and, finally, to propose a research plan to provide a knowledge base for making decisions on LWR plant life extensions.

Table 1. Comparison of ASTM chemistry specifications for cast stainless steels and their wrought equivalents [8,9].

Grade	Type	C max	Mn max	Si max	P max	S max	Cr	Ni	Mo	Nb	N
CF3	ASTM 743	0.03	1.5	1.5	0.04	0.04	17.0-21.0	8.0-12.0		---	
CF3A	ASTM 743	0.03	1.5	1.5	0.04	0.04	17.0-21.0	9.0-13.0	2.0-3.0	---	
CF3M	ASTM 743	0.03	1.5	1.5	0.04	0.04	17.0-22.0	9.0-13.0	2.0-3.0	---	0.10-0.20
CF8	ASTM 743	0.08	1.5	2.0	0.04	0.04	18.0-21.0	8.0-11.0			
CF8A	ASTM 743	0.08	1.5	2.0	0.04	0.04	18.0-21.0	8.0-11.0			
CF8M	ASTM 743	0.08	1.5	2.0	0.04	0.04	18.0-21.0	9.0-12.0	2.0-3.0		
304 SS	wrought SS	0.08	2.0	1.0	0.045	0.03	18.0-20.0	8.0-11.0	--	---	0.00-0.10
304L SS	Wrought SS	0.03	2.0	1.0	0.045	0.03	18.0-20.0	8.0-12.0	--	---	0.00-0.10
316 SS	wrought SS	0.08	2.0	1.0	0.045	0.03	16.0-18.0	10.0-14.0	2.0-3.0	---	0.00-0.10
316L SS	wrought SS	0.03	2.0	1.0	0.045	0.03	16.0-18.0	10.0-14.0	2.0-3.0	---	0.00-0.10
321 SS**	wrought SS	0.08	2.0	1.0	0.045	0.03	17.0-19.0	9.0-13.0	--	---**	0.00-0.10
347 SS	wrought SS	0.08	2.0	1.0	0.045	0.03	17.0-19.0	9.0-13.0	--	<1	0.00-0.10

(**0.70 wt% Ti)

2. BACKGROUNDS ON THERMAL AGING

2.1. Thermal aging embrittlement in duplex stainless steels

There has been a concern that the cast duplex stainless steel components in LWR systems can be susceptible to the thermal aging-induced embrittlement at reactor operating temperatures ranging from 280 to 320°C [1-7]. The thermal aging of cast stainless steels can cause an increase in strength, a decrease in ductility and fracture toughness and the ductile-brittle transition temperature shifts (ϕDBTT) to higher temperatures. Earlier investigations performed in Argonne National Laboratory [3-7] have suggested that the thermal embrittlement can occur in cast stainless steel components during the reactor design lifetime of 40 years. However, the majority of the earlier studies have been performed for aging response at temperatures higher than the common operating temperatures; i.e., the aging experiments have been often carried out in ócaccelerated agingô conditions to see detectable property changes within short periods. It has been customary to simulate the microstructural processes in aging during service temperatures by aging at or near 400 °C [5]. As a variety of aging mechanisms are reviewed below; however, we always need to be conscious on their relevance to the service conditions in LWR power plants.

For the CASSs, the degree of aging embrittlement depends on the grades and heats of the steels. As well summarized in the latest reports [3-7], the low carbon CF3 steels were generally more resistant to the thermal embrittlement than other alloys, while the Moï bearing, high carbon CF8M steels are the least resistant. Primary brittle fracture mechanisms observed in the thermally embrittled duplex stainless steels were the cleavage of ferrite and the separation of ferrite/austenite phase boundary. Indeed, the embrittlement is caused by changes in microstructure. For cast stainless steels, the main microstructural mechanisms of thermal aging at <500°C are associated with the precipitation of additional phases in the ferrite [3-7, 10-15]:

(a) formation of a Crï rich Ŭ phase through spinodal decomposition,
(b) nucleation and growth of Ŭ phase,
(c) precipitation of G phase (Ni, Si rich), $M_{23}C_6$ carbide, and ɔ$_2$ austenite,
(d) additional precipitation and/or growth of existing carbides at the ferrite/austenite phase boundaries.

While the thermal aging has little effects on the austenite phase, the formation of Crï rich Ŭ' phase by spinodal decomposition of ferrite phase is known to be the primary mechanism for thermal embrittlement [3-7, 10]. In steels, the martensite (Ŭ phase) particles harden the ferrite matrix but reduces the capability of plastic deformation before fracture as well as the cracking resistance in ferrite. In a ferritic-austenite duplex structure, the ferrite with extra hardening may fail in brittle mode but the surrounding austenite can provide some ductility. A highly embrittled case can be observed with a high contiguity of ferrite phase or with high ferrite content. Further, the ferrite/austenite phase boundary provides an easy path for crack propagation in highï C or highï N steels because of the excessive carbides or nitrides at boundaries [3,6].

The decrease in room temperature (RT) Charpy impact energy by thermal aging at 400°C [4ï 6,11,15,16] indicated that the RT impact energy reaches a minimum saturated value in all materials. The actual value of the saturation RT impact energy for a specific cast stainless steel is independent of aging temperature but depends strongly on the chemical composition of the steel; it is lower for the Moï bearing CF8M steels than for the Moï free CF3 or CF8 steels, and

decreases with an increase in ferrite content or the concentration of C or N in the steel.

The aging embrittlement progresses depending on many material and heating parameters such as chemistry of the material, processing conditions, and aging temperature [3-7]. The aging time at 400°C measured at the same reduction of impact energy in different heats varied by more than two orders of magnitude. In general, an aging mechanism with high activation energy can cause fast embrittlement, and the materials with the same chemical composition but different processing routes show different kinetics of embrittlement [6]. The cast stainless steels with low activation energy and slow embrittlement at 400°C show Gï phase precipitation after aging, and steels with high activation energy and fast embrittlement at 400°C do not contain a G phase [4-6, 10]. The primary embrittlement mechanism, spinodal decomposition of ferrite, should have higher activation because of the short range and fast characteristics of the process. The strengthening in ferrite is caused primarily by spinodal decomposition of ferrite to form the Crï rich Ŭ phase, and consequently the kinetics of thermal embrittlement should be controlled by the size and spacing of the Ŭ phase.

Except for the material conditions, aging temperature should be the most determining parameter for the kinetics of thermal embrittlement. Since the major aging mechanisms and their kinetics change with temperature, the activation energy for thermal embrittlement is not constant over the interested aging temperature range of 290ï 450°C [3-7]. It usually decreases with temperature, and the change is particularly steep between 400 and 450°C. It is known that the embrittlement will be non-existent or progresses very slowly in the reactor operating temperature range (280 ï 320°C). Consequently, data obtained after 450°C aging may not reflect the mechanisms that are active under reactor operating conditions, and extrapolation of the 450°C data to predict the extent of thermal embrittlement at reactor temperatures (280 ï 320°C) cannot be valid. The activation energy for thermal embrittlement may be represented by an average value in the temperature range of 290 ï 400°C [3,5].

2.2. Thermal Aging Considerations: Microstructural Processes

2.2.1. Overall on Thermal Aging Phenomena

The CASSs have optimized compositions and ferrite contents in order to promote improved strength, castability, corrosion resistance, and weldability. Because the CASS components are fabricated via relatively simple casting processes; however, the two ferrite and austenite constituents cannot be equally stable at elevated temperatures. It is anticipated, therefore, that the duplex nature of the alloys can create the different potential for thermal aging embrittlement in different portions through decomposition of existing phases and/or precipitation of new phases. Research should be focused on the aging conditions, temperature and time; where the CASS alloys are sensitive enough to observe thermal embrittlement, as well as where aging phenomena are relevant to the extended LWR service.

In the extended service at a high temperature, a variety of new phases may precipitate and lead to embrittlement as the new precipitates can harden the material and/or provide local crack initiation sites or propagation paths. Looking up microstructural processes which possibly lead to embrittlement is the primary goal of this review. A schematic of the time-temperature transformation plot is shown below in Figure 1, along with the potential influence of alloying elements on these curve shifts [14]. This figure indicates that two groups of phases will be formed as the CASSs age, depending on temperature range. The low temperature phase group

including G, ŭ, ŭ and ´ phases is more relevant to the reactor operation temperatures. Since the lower nose is formed around 450 °C (it depends on chemistry), the precipitation processes will be slower as the aging temperature becomes closer to the CASS component operation temperatures ~300 °C. Other phases such as h, ¿, R phases, carbides, and nitrides are formed in higher-temperature range. Also, indicated in the figure is that some elements accelerate these precipitation processes and thus expand the temperature-time area. In particular, the elements such as Cr, Mo, Cu, and W will accelerate process time as well as lower process temperature. Details for various phenomena are discussed below.

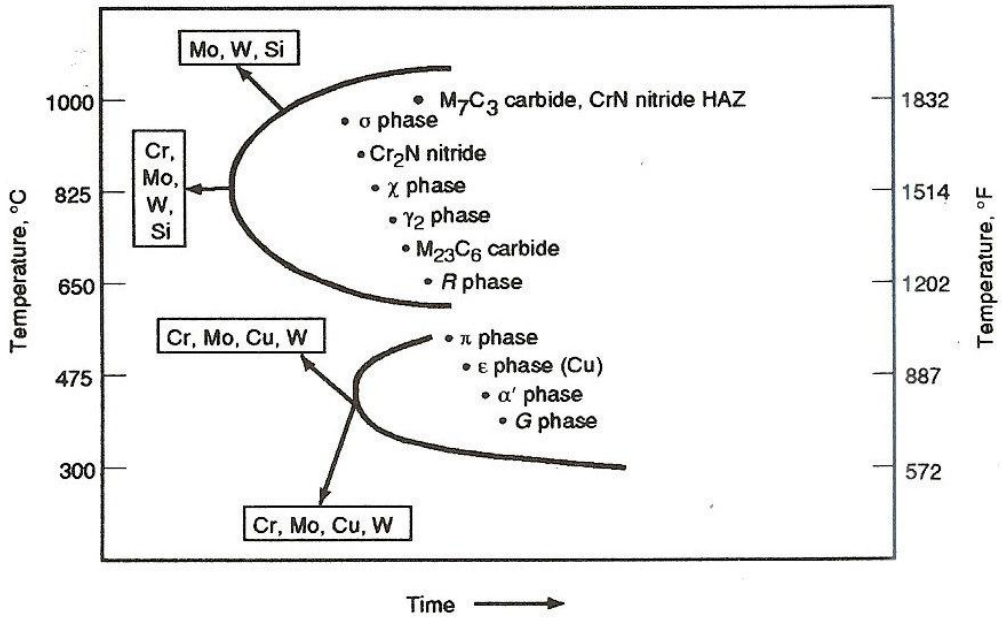

Figure 1. Time - temperature transformation diagram for CASS, showing the influence of alloying elements on precipitation reactions in duplex stainless steels [14].

2.2.1. Processes in Ferrite Phase [10-15]

Martensite (α') phase

The thermal aging embrittlement of CASS at temperatures below about 400°C arises primarily as a consequence of a thermally activated separation of chromium by diffusion in the Fe-Cr solid solution of the ŭ ferrite phase resulting in the formation of an iron rich Ŭphase and a chromium rich Ŭ phase. This process is called 'spinodal decomposition' and occurs mainly at the higher chromium contents greater than ~23% in the ŭ ferrite (for temperatures <400°C). The Ŭ phase may also form by precipitate germination and growth, particularly at temperatures >400°C, but can also contribute at lower temperatures depending on the precise combination of chromium content and temperature e.g. <~26%Cr at 400°C and <~23%Cr at 300°C.

The formation of Ŭ during thermal aging can affect all Fe-Cr solid solutions with Cr contents in solution >10%. An "oscillation" in the resulting Cr distribution is observed by high resolution microscopic techniques with wavelength (in order of nanometers) and amplitude increasing with aging time and temperature. The effect increases notably with the Cr and Mo content of the ferrite phase and consequently CF-8M is less resistant to aging than CF-8 or CF-3

without Mo. The formation of embrittling Ŭ phase from ŭ ferrite is enhanced by other alloying elements such as silicon which, together with Cr and Mo, can be represented by the chrome equivalent. The presence of the adjacent austenite phase in CASS appears to exert a detrimental influence relative to purely ferritic alloys of similar composition.

G phase

Other precipitation phenomena occur in the ŭ ferrite phase and at the ferrite-austenite interfaces above about 350°C, particularly the formation of the fcc Ni, Si, Mo rich G phase which can reach up to 12% by volume in Mo containing CASS. Carbon also enhances G phase precipitation. Nevertheless, the G phase does not appear to contribute significantly to hardening and loss of toughness. At higher temperatures between 400 and 500 °C other intermetallic phases precipitate but to a much lesser extent than G phase. However, extensive carbide (and sometimes nitride) precipitation, particularly at austenite-ferrite interfaces, occurs in the Mo-free CASS.

R Phase

The R phase is a Mo-rich intermetallic phase with trigonal crystal structure formed in the ferrite phase of duplex stainless steels or in the grain boundaries [15]. It is formed by a prolonged annealing at >550 °C, probably after sigma phase is formed. The formation of the Mo-rich phase may lead to rapid and significant loss of toughness.

π Phase

The ´ phase is nitride that has been found to precipitate intragranularly in the ferrite phase of 22Cr duplex stainless steel or in Mn-bearing austenitic stainless steel [15].

Activation Energy for Cr Diffusion

Although the microstructural evolution of CASS during thermal aging is fundamentally driven by solid-state diffusion processes, the complexity and changing nature of the phenomena with temperature is such that extrapolation over large temperature ranges using Arrhenius type relations is very difficult. Accelerated thermal aging for PWR and BWR applications is generally only carried out up to 400°C where hardening of the ŭ ferrite by Ŭ formation is the predominant aging process. Even with this restriction, the apparent activation energy observed for changes in mechanical properties such as hardness and toughness can be very variable and sometimes significantly below the activation energies of 210 - 260 kJ/mole associated with diffusion of metallic species, particularly Cr, in ferrite.

2.2.2. Processes in Austenite Phase and Boundaries [10-15]

Even the fully austenitic matrix of 316 SS is thermodynamically unstable [13,15]. During long-term exposure to elevated temperatures, the matrix will decompose into various carbide and intermetallic phases. These phases are often found at grain boundaries and other high-energy intragranular sites in the form of cubic or needle-like precipitates. In CASS, the austenite/ferrite boundaries may also serve as precipitation sites. These precipitates are responsible for the deterioration of mechanical properties, most notably a loss of ductility, following high temperature exposure.

The microstructural evolution of CASS during thermal aging is extremely complex: for

instance, one study identified at least 18 precipitate phases after exposure at 650°C [11]. However, many of these phases are also present in as-cast or annealed material that is ductile. Therefore, the majority of studies have focused on primary precipitate phases that are believed to significantly impact material properties. These include two carbide phases ($M_{23}C_6$ and MC_6) and three intermetallic phases (Laves or ɖ, ů, and ɢ).

Weiss and Stickler [12] developed time-temperature-precipitation (TTP) diagrams between the temperatures of 400 and 900°C and up to 3000 h. While these are at higher temperatures than LWR conditions, they are informative because LWR conditions will last hundreds of thousands of hours. Weiss and Sticker examined the effect of carbon content, solution treatment temperature, and cold work (CW) on the microstructural evolution of thermally annealed samples. The TTP diagram in Fig. 2 has been extrapolated to 100,000 h and altered to include the M_6C phase beyond 10,000 h observed by Stoter [11]. The TTP diagram for a low carbon (>0.03% C) stainless steel is shown in Fig. 3. Note that decreasing the carbon content (from ~0.07% in Fig. 2) significantly accelerates the formation of intermetallic phases, but reduces the formation of carbides. Figure 3 is a similar TTP diagram for cold worked material. Note that CW prior to aging accelerates the formation of carbide and intermetallic phases, an effect, which is attributed to increased diffusion.

In each of the three TTP diagrams, it is apparent that the $M_{23}C_6$ carbide phase forms first, while the intermetallic phases appear only after much longer aging times. At temperatures below 900°C, the austenitic matrix is supersaturated with carbon. This condition leads to the rapid precipitation of $M_{23}C_6$ carbides, often in a matter of minutes at the aging temperature. As the carbides form, the carbon content in the matrix decreases, which leads to the formation of the intermetallic phases ɖ, ů, and ɢ. Once the intermetallic phases form, the austenitic matrix is depleted of chromium and molybdenum, which increases the solubility limit of carbon and often leads to the resolution of the $M_{23}C_6$ carbide precipitates.

Some general trends have been noted for the majority of precipitate phases. Thermal aging at higher temperatures causes precipitate particles to be coarser, whether on a grain boundary or intragranularly. Smaller grains result in phase instability because they provide additional nucleating sites and decrease diffusion paths for precipitate forming elements [13].

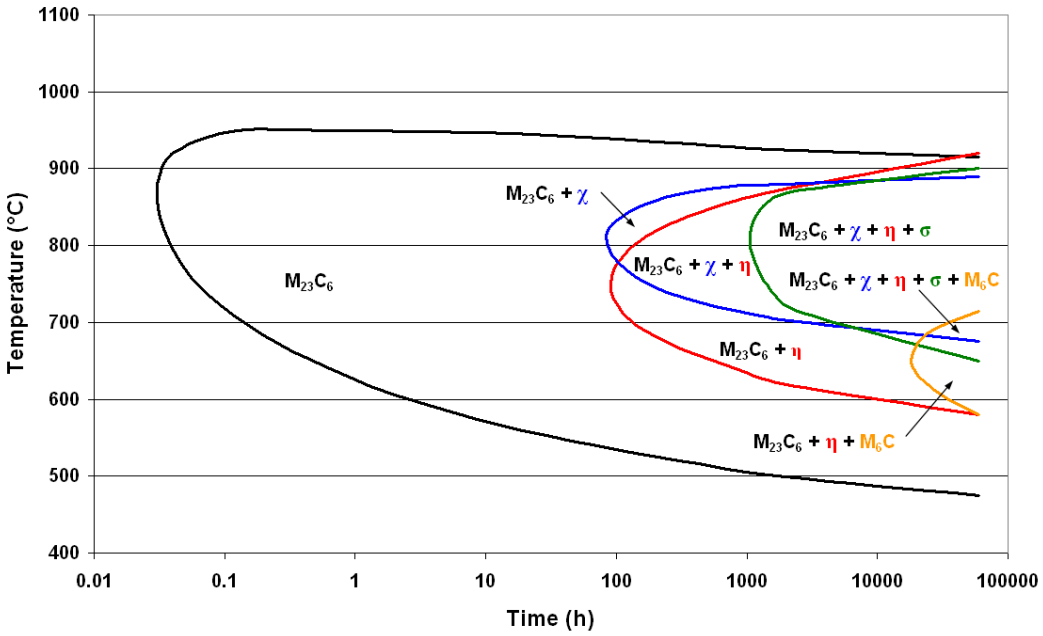

Fig. 2. TTP diagram of CASS during thermal aging [11].

M_6C Carbides

The M_6C precipitate is not very common in austenitic stainless steels. Weiss and Stickler observed M_6C in low carbon 316L for aging times of ~3000 h, but not for 316 with a higher carbon content [11]. Stoter identified M_6C after long-term aging (>28,000 h) at 650°C. M_6C is a diamond type face-centered cube carbide. It is usually associated with very large $M_{23}C_6$ precipitates and has widely variable composition (with the exception that there is always 1% vanadium present). M_6C precipitates are predominantly found along grain boundaries and at triple point junctions [12].

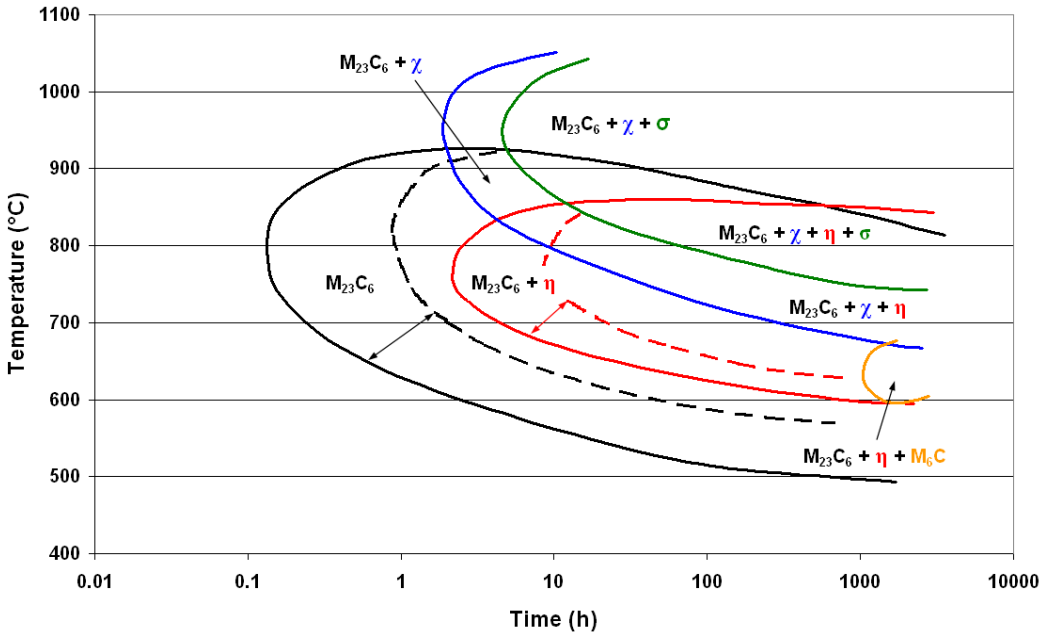

Fig. 3 TTP diagram of low C CASS during thermal aging [11]. Dashed lines represent a lower solution anneal temperature (1090°C versus 1560°C).

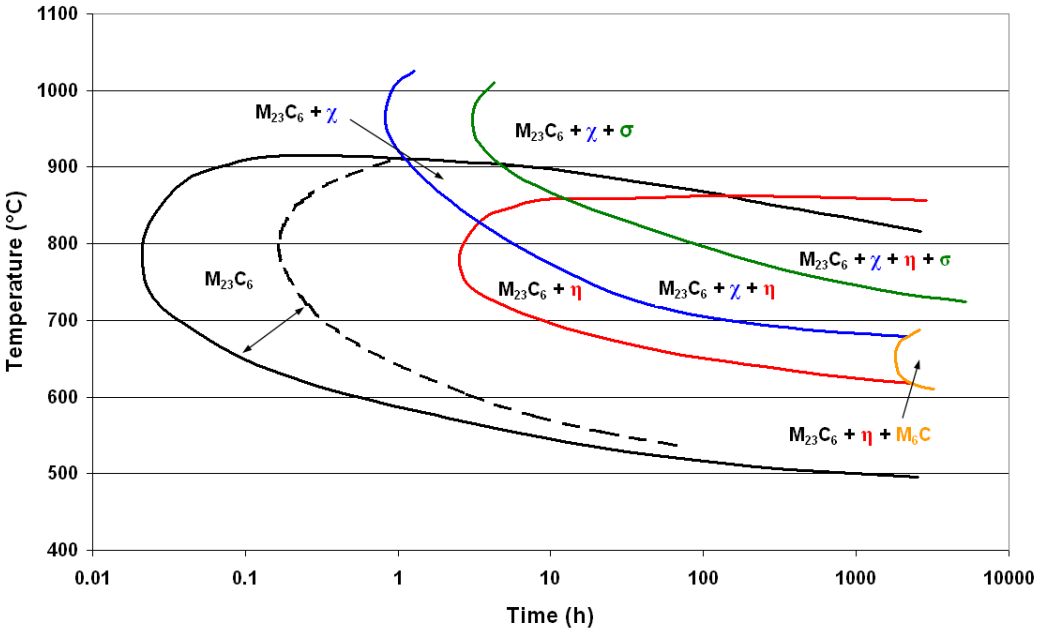

Fig. 4 TTP diagram of cold worked SS during thermal aging[12]. Dashed line represents a lower solution anneal temperature (1090°C versus 1260°C).

$M_{23}C_6$ Carbides

The most dominant precipitate in CASS is the $M_{23}C_6$ carbide phase, where the metal atom (M) is most likely to be chromium [10.15]. The lattice parameters of face-centered cubic $M_{23}C_6$ tend to increase with aging temperature and time, reflecting an increase of the molybdenum content of the carbide [12]. The $M_{23}C_6$ carbide tends to precipitate successively on grain boundaries, incoherent twin boundaries, coherent twin boundaries, and intragranularly. The precipitates on grain boundaries are large and the number of precipitates increases with boron content [10,15]. Aging at 650°C produces a uniform distribution of cubic precipitates on intragranular dislocations, while aging at higher temperatures resulted in large bulky precipitates on the grain boundaries with little precipitation intragranularly [12]. Cold working causes the $M_{23}C_6$ precipitates to form almost as readily at deformation bands as at grain boundaries [10].

Solution annealing at higher temperatures results in a larger $M_{23}C_6$ carbide size (as shown in Fig. 3). High temperature annealing produces larger grains, which present a smaller volume of grain boundaries for precipitate formation. This, coupled with the higher quenched-in vacancy formation, results in higher solute-segregation along grain boundaries. Therefore, a shorter aging time is required for $M_{23}C_6$ precipitation.

The precipitation of $M_{23}C_6$ is generally not desirable for good creep properties, except in the fine intragranular form. Also, $M_{23}C_6$ is often associated with intergranular corrosion since its formation causes a local depletion of chromium along grain boundaries, thus losing the desirable ñstainlessò property on a local scale [10].

Sigma (σ) Phase

The sigma (ů) phase is a well-known intermetallic precipitate in Fe-Cr material systems that are often associated with embrittlement. Sigma phase is a tetragonal crystal composed of $(Cr,Mo)_x$ $(Ni,Fe)_y$. There are several theories concerning the formation of ů phase [16], but it always requires a high-energy interface to form. As expected, ů phase precipitates successively appear at triple points, grain boundaries, twin boundaries, and intragranularly at oxide inclusions. There is some evidence that the ů phase precipitates only form on previous $M_{23}C_6$ sites or grow where $M_{23}C_6$ precipitates are dissolving [12]. The formation of ů phase can be retarded by solution annealing at high temperatures because the larger grains present a longer diffusion path for ů-forming elements to reach the grain boundaries. By contrast, cold working accelerates ů phase formation due to increased diffusion rates. However, it was found that recrystallization of the cold worked microstructure had much greater impact on the amount and timing of the ů phase formation than did CW alone [13]. The ů phase has a detrimental effect on creep properties when located at grain boundaries, but little effect when it precipitates intragranularly [10].

Chi (χ) Phase

The chi (ɢ) phase is a body centered cubic crystal that is typically thought of as a carbon-dissolving compound that behaves as either an $M_{18}C$ carbide or an intermetallic. A typical composition is $Fe_{36}Cr_{12}Mo_{10}$ and the metallic contents are highly exchangeable [10,15]. The nucleation of ɢ phase typically follows the order of grain boundary, twin boundaries, and intragranular. The morphology of ɢ phase varies from large globular particles to rod-shaped crystals. Although a higher solution temperature will decrease the size of ɢ phase particles, it does not decrease the number of particles. Cold working causes ɢ-phase to precipitate within the matrix of the material in rod-shaped particles.

Laves (η) Phase

Laves (ɖ) phase particles are hexagonal crystals that are composed of Fe_2Mo in many molybdenum-containing alloys. Laves phase is often found as small equiaxed particles intragranularly, and occasionally found on the grain boundaries [10,15]. High temperature annealing (above 1400°C) is effective at retarding the development of Laves phase particles because ŭ-ferrite forms, which favors the production of sigma and chi phases. Cold working accelerates Laves phase formation due to increased diffusion rates. These phases are considered detrimental to ductility and fracture toughness, while their effects on creep and high temperature deformation are not certain.

2.3. Other Considerations

2.3.1. General Corrosion

General (uniform) corrosion of CASS alloys is well studied and corrosion rates are typically very low, which is a prime driver for their use in this application. To date, there are no known service problems with CASS in the area of general corrosion. Under extended service conditions, additional time will lead to increased corrosion (weight loss or wall thinning); however, the rate of corrosion is so slow that this is unlikely to increase risk of component failure. The potential effects of thermal aging could lead to increased corrosion effects and this should be evaluated.

2.3.2. Localized Corrosion/Pitting

As with general corrosion, localized corrosion or corrosion of CASS alloys is well studied and not a concern in modern LWR water chemistries. To date, there are no known service problems with CASS in the area of pitting or localized corrosion. Under extended service conditions, additional time will lead to increased exposure to the coolant although pitting of CASS is unlikely to be a concern to service.

2.3.3. Flow Accelerated Corrosion

There are no known instances of flow-accelerated corrosion problems in todayôs fleet for CASS components. This is the expected behavior for these alloys. As above, while extended service conditions will lead to increased exposure to the coolant although pitting of CASS is unlikely to be a concern to service.

2.3.4. Stress Corrosion Cracking (SCC)

Stress corrosion cracking has been observed in several cases in CASS in nuclear applications in both BWR and PWR environments. However, these observations are very limited [10]. In those cases, analysis of the cracked components revealed that the material was either higher in C or lower in ferrite than specified, leading to increased susceptibility. There have also been limited observations of SCC in weldments of CASS components. However, as above, these have been attributed to improper heat treatment and/or cold-working rather than a

general susceptibility.

Stress-corrosion cracking of CASS has been identified as a knowledge gap in the most recent versions of the EPRI MDM and Issue Management Tables [11]. As noted in the MDM, this ñis not intended to denote a significant concern at present, but rather to communicate the current lack of susceptibility data for CASS materials. A possible area warranting additional investigation is the potential effect of long-term thermal aging on the SCC susceptibility of CASS components having high ferrite content, considering that other materials (i.e. martensitic stainless steels) that embrittle with age also exhibit increased SCC susceptibility.ò

SCC of CASS components under extended service: The positive service performance of CASS materials to date is encouraging when considering extended service conditions. However, the lack of susceptibility data for SCC and the potential influence of long-term aging may drive phase transformations must be considered. Thermal aging, as described above, could lead to increased SCC susceptibility. Additional studies on the dominant phase transformations and potential impacts on susceptibility are warranted.

2.3.5. Irradiation Effects

The evaluation of irradiation-induced degradation is a critical step in validating material service under any conditions. Nuclear reactor systems impose a harsh environment and radiation damage conditions on structural materials. While the exact materials and degradation mechanisms vary between the different applications, the fundamentals of radiation damage are the same. Irradiation of materials in reactors can lead to extensive changes in microstructure, micro-composition, and macroscopic properties.

Neutron irradiation can produce large property and dimensional changes in materials, primarily via one of five radiation damage processes: (i) radiation-induced hardening and embrittlement (occurring predominantly at low exposure temperatures); (ii) phase instabilities from radiation-induced or -enhanced segregation and precipitation; (iii) irradiation creep due to unbalanced absorption of interstitials vs. vacancies at dislocations; (iv) volumetric swelling from cavity formation; and (v) high temperature helium embrittlement due to formation of helium-filled cavities on grain boundaries.

The key challenge for materials performance is to identify key degradation modes based on past history and exact irradiation conditions. For CASS; however, the irradiation effects are a minor concern in todayôs BWR fleet. Irradiation-induced hardening is the primary form of degradation associated with cast stainless steels and is closely related to the sensitivity to embrittlement observed in reactor pressure vessel materials. Currently, CASS components are limited to a maximum fluence of 1×10^{19} n/cm^2. This limit was established by the BWRVIP program [17] to limit the potentially deleterious effects of radiation-induced hardening. To date, there are no reports of irradiation-induced degradation limiting operation of these components.

Clearly, extended service conditions will increase the total fluence to CASS components, although the total fluence will depend on a number of factors unique to each plant and location (e.g. location, lifetime, power-uprates, etc.) Careful consideration of maximum fluence and relation to the BWRVIP is warranted.

As noted above, the effects of irradiation on phase transformations and hardening may have synergistic effects on other forms of degradation. The potential influence of irradiation-induced hardening and loss of fracture toughness may impact stress-corrosion cracking susceptibility, analogous to that in wrought stainless steel components. In addition, the impact of

irradiation-enhanced diffusion on thermal aging processes could accelerate that form of embrittlement.

2.3.6. Fatigue

As with general and localized corrosion, there are no known instances of fatigue problems in today's fleet for CASS components. Under extended service conditions, components will experience longer lifetimes and additional cycles and, as with most materials, fatigue and environmental fatigue could become a greater concern simply due to the longer service life.

As with previous sections, the largest uncertainty in fatigue behavior may be the result of synergistic effects related to thermal aging. If phase transformations occur under extended lifetimes, loss of fracture toughness could lead to increased concerns with fatigue and environmental fatigue.

2.4. Summary and Concerns

The cast stainless steels are important materials in modern LWR facilities. Today's fleet has experienced very limited failures or material degradation concerns. In the limited number of service observations of degradation, all have been attributed to some abnormal characteristics due to high carbon content, low ferrite content, or improper processing.

It was recognized that significant property degradation by thermal aging has been reported only when aging temperature was significantly higher than reactor service temperature. An accelerated aging near or at 400 °C can easily cause embrittlement within a time frame much shorter than current reactor lifetime. Under extended service scenarios, there may be degradation modes to consider for the CASSs and components at temperatures much closer to operation temperatures. A prolonged thermal aging could lead to decomposition of key phases and formation of other deleterious phases. Such aging could result in the loss of fracture toughness (analogous to that observed in other martensitic stainless steels). Additional surveys of potential phase changes and aging effects would help reduce uncertainty of these mechanisms.

While there have been extended researches for CASS aging phenomena, little effort has been made to connect macroscopic measurements with the kinetics of microstructural processes. The activation energies, for example, have been measured from mechanical property changes such as hardness, which actually include mixed effects from various microstructural mechanisms. The activation energies measured by mechanical properties may result in large uncertainties in mechanistic studies and thus reduce the predictability of aging effects for extended lifetime.

Other forms of degradation such as general corrosion, localized corrosion, flow-accelerated corrosion, stress-corrosion cracking, irradiation effects, and fatigue are not expected to limit operation under extended service conditions based on performance in the fleet to date. However, the synergistic effects of long-term thermal aging on these other forms of degradation must be considered in greater detail.

2.5. References

[1] MDM and PWR IMT, 2010.

[2] Cracking observations in CASS
[3] O. K. Chopra and A. Sather, ñInitial Assessment of the Mechanisms and Significance of Lowï Temperature Embrittlement of Cast Stainless Steels in LWR Systems,ò NUREG/CRï 5385 (ANLï 89/17) (1990).
[4] H. M. Chung and T. R. Leax, ñEmbrittlement of Laboratoryï and Reactorï Aged CF3, CF8, and CF8M Duplex Stainless Steels,ò *Mater. Sci. Technol.*, **6**, 249ï 262 (1990).
[5] H.M. Chung, ñEvaluation of Aging of Cast Stainless Steel Components,ò *ASME Pressure Vessel & Piping Conference*, San Diego, CA, June 23-27, (1991).
[6] O. K. Chopra, Estimation of Fracture Toughness of Cast Stainless Steels during Thermal Aging in LWR Systems, NUREG/CRï 4513 (ANLï 90/42) (1991).
[7] W.F. Michaud, P.T. Toben, W.K. Soppet, O.K. Chopra, Tensile-Property Characterization of Thermally Aged Cast Stainless Steels, NUREG/CR-6142 (ANL-93/35) (1994).
[8] Standard, ASME/ASTM SA/A 743/A 743M, ñSpecification for Castings, Iron-Chromium, Iron-Chromium-Nickel, Corrosion-Resistant, for General Application.ò
[9] Standard, ASME/ASTM SA/A 744, ñSpecification for Castings, Iron-Chromium-Nickel, Corrosion Resistant, for Severe Service.ò
[10] T. Sourmail, ñPrecipitation in creep resistant austenitic stainless steels,ò *Materials Science and Technology,* 17 (2001) 1.
[11] L.P. Stoter, ñThermal ageing effects in AISI type 316 stainless steel,ò *Journal of Materials Science,* 16 (1981) 1039.
[12] B. Weiss and R. Stickler, ñPhase Instabilities during High Temperature Exposure of 316 Austenitic Stainless Steel,ò *Metallurgical Transactions* 3 (1972) 851.
[13] J.E. Spruiell, et al., ñMicrostructural Stability of Thermal-Mechanically Pretreated Type 316 Austenitic Stainless Steel,ò *Metallurgical Transactions* 4 (1973) 1533.
[14] J. Charles "Super Duplex Stainless Steels - Structure and Properties" in *Proceedings of Duplex Stainless Steel Conference*, Vol 1, Les Editions de Physique, Les Ulis Cedex,(October 1991) pp. 3-48.
[15] K.H. Lo, C.H. Shek, J.K.L. Lai, ñRecent developments in stainless steels,ò *Mater Sci Engineer R* 65 (2009) 39-104.
[16] J. Barcik, *Materials Science and Technology*, 4 (1988) 5.
[17] BWRVIP guidelines on cast stainless steel.

3. RESEARCH PLAN

3.1. Objective

The final goal of this work is to provide knowledge-based conclusive prediction for the integrity of the CASS components of LWR power plants during the service life extended up to and beyond 60 years.

3.2. Aging Time Calculation

Determining aging temperatures and periods is the first step in the thermal aging research for CASS, and therefore, a basic calculation has been performed to approximately scope the aging temperature and time for the proposed research. Since it is practically not possible to pursue a real-time aging experiment for the extended life time of 60 years or more, an accelerated aging experiment will be carried out for a time frame of five years or so. A key principle in choosing the aging temperature and time should be that the aging mechanisms at the elevated temperatures must not differ from those found in the service temperature range of 280 ï 320 °C. Therefore, the test (aging) temperatures need to be as close to the service temperature as possible.

At elevated temperatures the microstructural aging mechanisms are thermally activated and the kinetics of each mechanism should be controlled by its activation energy. Any apparent activation energy, if measured by a macroscopic property, is considered as the average of multiple activations corresponding to so many mechanisms. Even if the same aging mechanisms occur in both the service and the accelerated aging experiment, therefore, the relative roles of those mechanisms can be different and thus the average activation energy changes with aging temperature. It is also worth noting that the activation energies measured by changes in mechanical properties such as hardness and toughness may not accurately reflect real microstructural progresses in CASS because those macroscopic properties can include both negative and positive effects from aging processes. Some precipitation mechanisms, for example, may soften the material, which generally helps increase fracture toughness, but provide new crack initiation sites. Recognizing that these complexities can lead to significant uncertainties in determining accelerated-aging temperatures, a wide range of temperatures are included in this research, while a few aging temperatures will be selected to generate realistic data based on the reasoning from the following calculation.

In calculation, the aging time for experiment is determined to simulate the 60 or 80 years of aging in plant service. To calculate the aging time t(T) in accelerated aging experiment at an elevated temperature T, the Arrhenius type equation is used [5]:

$$t(T) = t_0 \times e^{Q/RT_0 - Q/RT}$$

where t_0 and T_0 are the time and temperature for service lifetime, respectively, and Q is the activation energy (in kJ/mole) and R the gas constant (8.3144621 J/mole.K). The t_0 was set at 60 or 80 years and T_0 at 300 °C. Calculation has been performed for a wide range of activation energy, 50 ï 300 kJ/mole, to take into account any possible aging mechanisms. As mentioned earlier, the activation energies for diffusion of metallic elements in ferrite phase are in the range

of 210 ï 260 kJ/mole. This should approximately represent the spinodal decomposition process to form ŬNjind Ŭphases, which is considered the most responsible embrittle mechanism in CASS aging. Much lower activation energies (50 ï 150 kJ/more) are included to consider possibly low apparent activation energies measured by macroscopic property changes.

Figures 5 and 6 display the aging time versus aging temperature curves in semi-log coordinate in accelerated aging experiment to simulate, respectively, 60 and 80 years of services. These state that the temperature dependence of aging time varies widely with activation energy. In Fig. 5, for a mechanism with the activation energy of 240 kJ/mole, for example, a CASS needs to be aged at about 330 °C, a 30 °C increase from the representative service temperature (300 °C), to complete the simulated aging for a service of 60 years in 5 years; aging at about 377 °C for 5 years is needed for the mechanism with an activation energy of 100 kJ/mole. These aging temperatures will be shifted by the same amount as the change in service temperature in calculation. A rectangular band marked at 5 years is to range the aging temperature for the aging mechanisms caused by the diffusion of metallic elements: 328 ï 334°C is the aging temperature range for 210 ï 260 kJ/mole. It is easily seen in Fig. 6, which simulates an 80 year service at 300 °C, that these aging temperatures are shifted by about +5 °C from those in Fig. 5; the aging at 335 °C for 5 year simulates the 80 year service as indicated at the middle of rectangular band.

In determining the aging temperatures for simulation experiment, four aging temperatures can be first selected to represent the wide range of activation energy: (a) the service temperature 300 °C needs to be included to represent CASS service temperature range 280 ï 320 °C. Although the aging at this temperature cannot simulate extended lifetime aging at service, the experimental results can be used to validate the current approach or, at least, to provide reference data for comparison with the results from shorter term aging at higher temperatures, (b) the middle temperature in the rectangular band, 330 °C (or 335 °C), should be included to simulate seemingly most probable aging mechanism of spinodal decomposition which involves metallic element diffusion, (c) aging at 400 °C is believed to cover very slow aging mechanisms with activation energies of 50 ï 100 kJ/mole, as indicated in Figs. 5 and 6. Traditionally, this temperature has been selected for many accelerated aging experiments, and (d) finally, at least one temperature between 330 °C and 400 °C, mostly likely 360 °C, will be added to the aging temperature select.

These four aging temperatures ranging from 300 to 400 °C are believed to cover all possible aging mechanisms needed to explain phenomena in service conditions. Although the highest temperature, 400 °C, has been often selected for accelerated aging, there is no convincing comparison of mechanisms and kinetics that shows aging at 400 °C can accurately simulate the aging phenomena at about 300 °C. The validation of the accelerated aging practices will be therefore one of the main goals of this research.

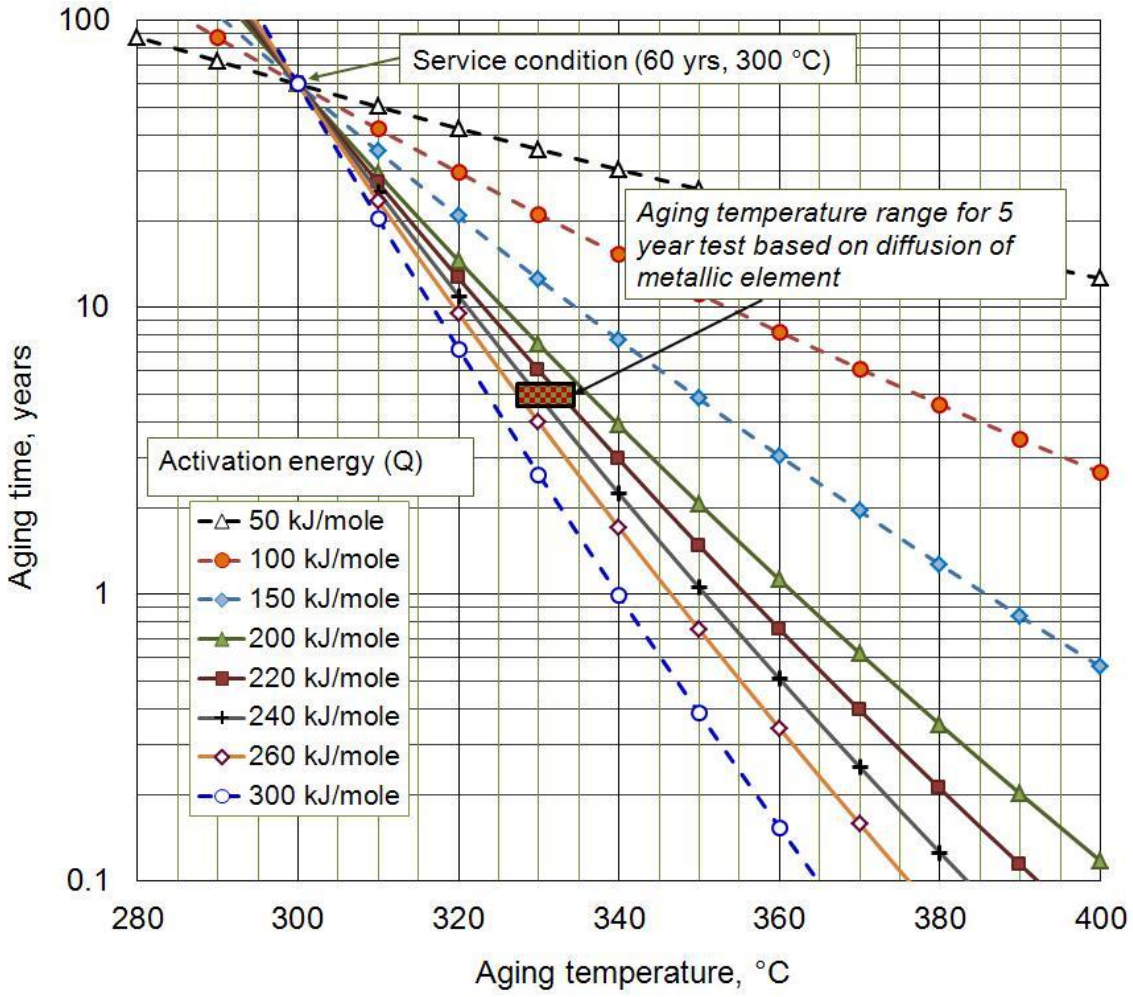

Fig. 5. Semi-log plot of aging time versus aging temperature curves for different activation energies. Note that the aging time is defined to simulate 60 year service at 300 °C in accelerated (higher temperature) aging experiment.

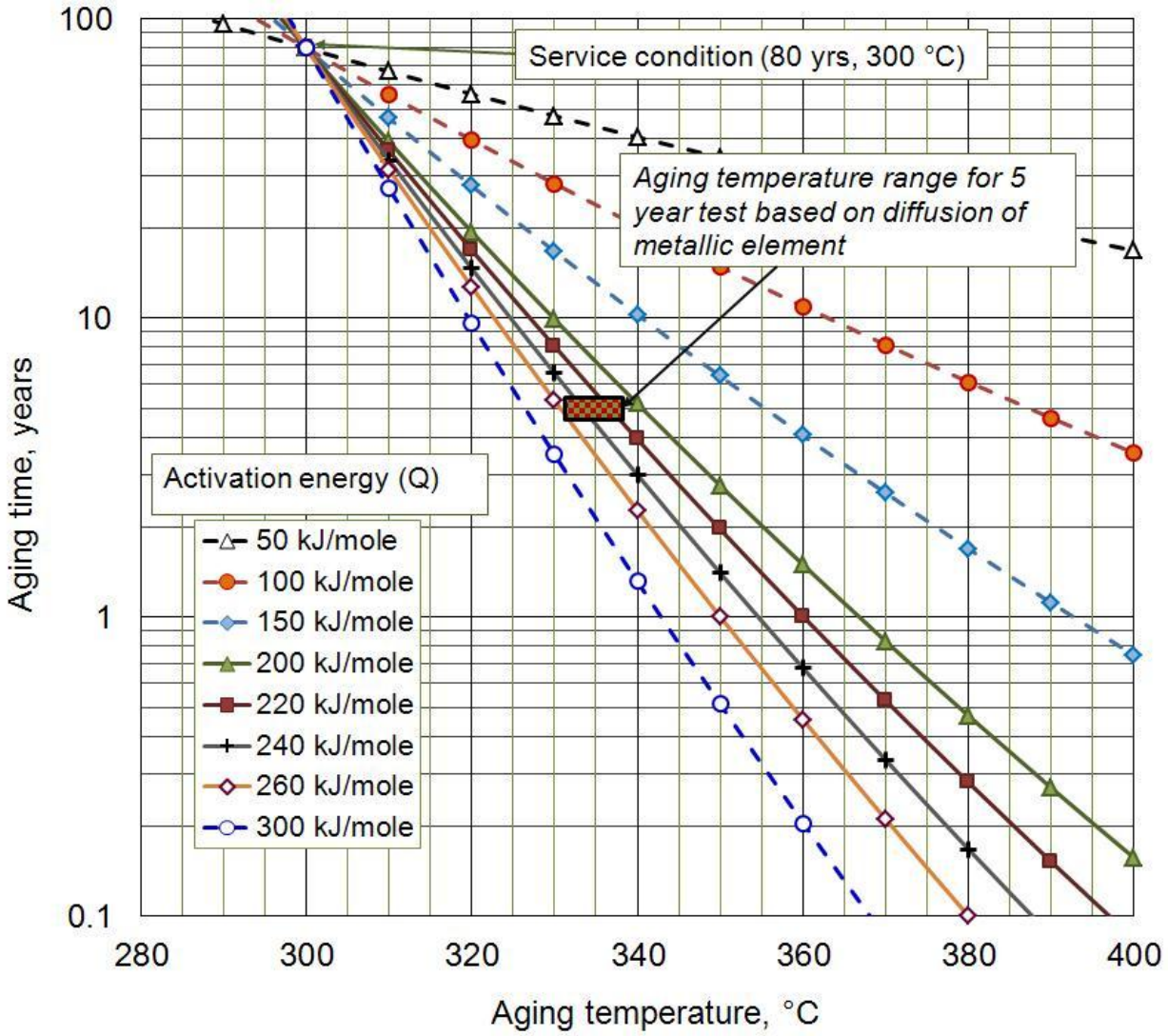

Fig. 5. Semi-log plot of aging time versus aging temperature curves for different activation energies. Note that the aging time is defined to simulate 80 year service at 300 °C in accelerated (higher temperature) aging experiment.

3.3. Technical Tasks/Research Activities

3.3.1. Task 1: Long-term aging treatment and model prediction

Accelerated aging experiments will be performed to provide aged CASS specimens for mechanical tests and microstructural analyses. This aging experiment plan will focus on building a sufficient knowledge base within a limited time of five years or so. As suggested above, the final aging treatment schedules will be determined using the result of activation energy based calculation for diffusion and/or precipitations. Specimens will be aged at elevated temperatures higher than service temperatures to accelerate aging effect in the cast stainless

steels. Duration of aging treatments will range from 6 months for the shortest to about 5 years for the longest.

Post-aging characterization will include (a) basic mechanical (tensile, hardness) tests, (b) static and dynamic fracture toughness tests, and (c) microstructural examinations including TEM, atom probe, and SEM for selected specimens. Specimens for these tests and examinations will be machined, sealed in stainless steel foil envelopes, and aged in furnaces. At least 5 specimen packages are produced for each aging temperature for yearly retrievals. Baseline examinations will be carried out in the first year for non-aged material. One fifth of specimen packages (or four packages aged at four different temperatures) will be removed from furnaces every year and specimens will be tested. Future aging schedule will be re-evaluated considering the latest test results as well as computational study results. Specimen removals and any furnace heating-cooling activities will be recorded; furnace temperatures will be recorded periodically.

3.3.2. Task 2: Mechanical testing and evaluation of aged cast stainless steels

Mechanical testing and evaluation aims at quantifying the effect of simulated aging on cast stainless steels. The main output will be the mechanical property database used to simulate and predict the behaviors of the cast stainless steels during extended plant operation. The mechanical testing is a yearly campaign as the specimen packages are removed yearly from furnaces. The mechanical testing includes tensile and hardness tests for strength and ductility data and static and dynamic fracture tests for fracture toughness data. The aged specimens will be also used for other types of mechanical tests and analysis if determined to do so based on the tensile and fracture test results.

Integration of mechanical property, microstructural characterization, and simulation data will lead to prediction correlations for property changes during extended operation. The prediction correlations will be developed as mechanism-based functions, in which both the microstructural aging mechanisms and the deformation and failure mechanisms are taken into account.

3.3.3. Task 3: Microstructural evolution analysis

Microstructural evolution and elemental redistribution behaviors during aging will be analyzed in detail to explain the property changes as well as to provide feedbacks and knowledge base for future material selection and processing for CASS components. For selected aging conditions, phase changes and precipitation behaviors are analyzed using various methodologies including TEM, SEM, Atom Probe, etc. Elemental segregation and diffusion behaviors are also analyzed for aged specimens since ageing treatment at relatively low temperatures is believed to induce elemental redistribution even without observable phase change or precipitation. Embrittlement at operation temperature (<350), if any, is believed to be due to microscopic phenomena such as localized phase decomposition, elemental segregation, and fine precipitation. Such slow, long-term phenomena, especially at grain boundaries and interfaces, will be studied to correlate with other property changes. It will be also attempted to validate the accelerated aging approach by comparing microstructural processes at service and elevated aging temperatures.

The response of a material to mechanical loading is always related to the microstructure of the material. To explain the mechanical properties of aged CASS and to provide means for

predicting behaviors of components in possible loading schemes during service, deformation and fracture mechanisms are studied for selected aged materials: detailed analyses on microstructure and elemental distribution in aged and deformed or fractured specimens are performed. Special loading method will be developed if any loading scheme in operation is identified but is not represented by the planned mechanical tests.

3.3.4. Task 4: In-situ testing and validation

In-situ test data will be obtained from operational parts in power plants or from the material taken from parts in past power plants to validate the property data produced after the accelerated aging treatments. The primary method to collect mechanical data is ball indentation testing, which can produce strength and strain hardening data from a very small volume. The ball indentation testing is often called semi-nondestructive method since it leaves only small indents (<1 mm in diameter) on tested surface. Also, if available, microstructural data will be obtained from those plant-aged materials/components and compared with those from furnace-aged CASSs. Existing data are also collected and reanalyzed based on results of mechanism studies.

3.3.5. Task 5: Computational study on long-term aging phenomena

Computational study on long-term thermal aging phenomena is performed to strengthen experimental results and to further understand the aging related phenomena. The phenomena which cannot be easily observed by experimental means will be searched for in this task. This task is expected to simulate the details of precipitation, phase decomposition, and segregation phenomena.

For selected alloys, the kinetics of individual aging mechanisms such as formation of ŬNj and Ŭphases, carbide formation, and diffusion/segregation will be calculated to produce information on phase transformation behaviors such as TTP diagram. Calculation of physical data for aging mechanisms such as activation energies will be carried out to provide feedbacks to the present accelerated aging approach.

3.3.6. Work flow in aging research

A schematic of work flow in the research package is displayed below. Various types of specimens will be aged at different temperatures based on the aging treatment schedule determined by the model calculation above and provided to the mechanical property and microstructural change studies. Computational studies will be performed using input data from microstructural examinations to confirm/explain the results of microstructural observation on aging phenomena. The in-situ testing data from used components or in-service facilities will provide confirmation for mechanical test data from the accelerated aging experiment. All of the results from these activities will be integrated and analyzed to generate knowledge base for CASS aging phenomena and final conclusive recommendation for extension of plant life time.

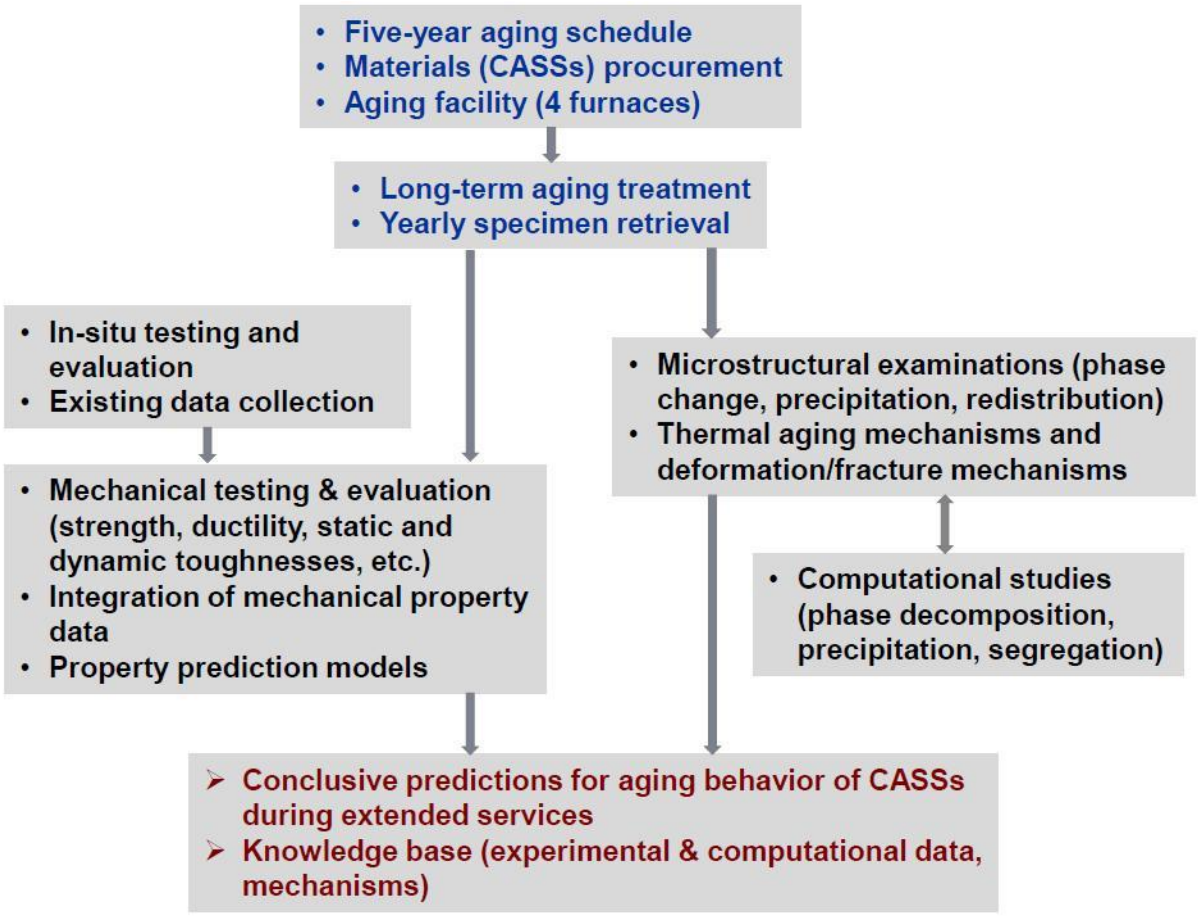

Figure 6. Work flow of CASS thermal aging research

3.4. Research Schedule

Table 2 lists subtasks and corresponding work schedules, which correspond to the descriptive activities under tasks 1 ï 5 in previous section. The outputs of these tasks are listed in the next section 3.5 as yearly deliverables. Added in the table is the task 0 for work package management, which includes the planning, data integration, and reporting activities by PI. While the majority of subtasks are initiated in FY 2013, planning (this document) and preparation of furnaces has been already performed for a few months in FY 2012. The start of computational simulation task will be in FY2014.

Table 2a. Research Schedule for Cast Stainless Steel Thermal Aging (Tasks 0 – 2)

Tasks/Activities	Lead	2012		2013		2014		2015		2016		2017	
0. Planning, Integration, Reporting	Byun												
• 5-year plan													
• Integration, reporting and publication													
• Final report/conclusion													
1. Long-term aging treatment and model prediction	Byun												
• Model calculation for aging condition													
• Procurement of materials													
• Aging facility/maintenance													
• Machine specimens/start aging treatment													
• Retrieve aged specimen packages/aging schedule adjustment													
2. Mechanical testing and evaluation of aged cast stainless steels	Byun												
• Baseline testing for pristine materials													
• Tensile & hardness tests of aged specimens													
• Static fracture (J-R) tests													
• Dynamic fracture tests (Cv or precracked)													
• Integration of property data & development of property prediction models													

Table 2b. Research Schedule for Cast Stainless Steel Thermal Aging (Tasks 3 – 5)

Tasks/Activities	Lead	2012		2013		2014		2015		2016		2017	
3. Microstructural evolution analysis	Leonard/ Postdoc												
• Precipitation/phase decomposition analysis (TEM/Optical/others)													
• Deformation & fracture mechanism study													
4. In-situ testing and evaluation	Byun/ Postdoc												
• Technique development/equipment setup													
• In-situ testing													
• Data analysis/assessment of accelerated aging data													
5. Computational study on long-term aging phenomena/embrittlement	TBD												
• Precipitation/phase decomposition													
• Segregation/diffusion													

3.5. Deliverables

FY	Deliverables
2012	• Five-year plan (with a summary on thermal aging ï this document)
2013	• Report on mechanical testing and microstructure examination results for aged materials (year 1 &2) • Baseline data by semi-nondestructive testing technique • Completion of computational study tools and preliminary ageing simulation results
2014	• Report on mechanical testing and microstructure examination results for aged materials (year 1 &2) • Baseline data by semi-nondestructive testing technique • Completion of computational study tools and preliminary ageing simulation results
2015	• Intermediate report on in-situ mechanical test data • Intermediate report on computational study (methodology and intermediate results) • Mechanical testing and microstructure examination results for aged materials (year 3) • Research paper(s)
2016	• Report on mechanical testing and microstructure examination results for aged materials (year 3 &4) • Completion of in-situ mechanical tests • Completion of major computational analyses • Research paper(s)
2017	• Final report on mechanical testing and microstructure examination results for aged materials (years 1 ï 5) • Final report on in-situ mechanical property data • Concluding report on cast stainless steel aging integrating key mechanical, microstructural, computational analyses results • Research paper(s)

3.6. Proposed Budget Plan

(Budget in k$)

Task/activities	P.I.	2012	2013	2014	2015	2016	2017
0. Planning, Integration, Reporting	T.S. Byun	85	70	70	70	70	70
· 5-year plan							
· Integration, reporting							
· Final report/conclusion							
1. Long-term aging treatment and model prediction	T.S. Byun	40	140	60	60	60	60
· Model calculation for aging condition							
· Procurement of materials							
· Aging facility/maintenance							
· Machine specimens/start aging treatment							
· Retrieve aged specimen packages/aging schedule adjustment							
2. Mechanical testing and evaluation of aged cast stainless steels	T.S. Byun		80	140	150	150	150
· Baseline testing for pristine materials							
· Tensile & hardness tests of aged specimens							
· Static fracture tests (J-R) tests							
· Dynamic fracture tests (Cv or precracked)							
· Integration with microstructural and computational study results							
3. Microstructural evolution analysis	K. Leonard		60	80	90	90	90
· Precipitation/phase decomposition analysis (TEM/Optical)							
· Deformation & fracture mechanism study							
4. In-situ testing and evaluation	T.S. Byun		150	70	70	70	100
· Technique development/equipment setup							
· In-situ testing/planted-aged materials testing							
· Data analysis/assessment of accelerated aging data							
5. Computational study on long-term aging phenomena/embrittlement	(tbd)			80	80	80	50
· Precipitation/phase decomposition							
· Segregation/diffusion							
Sum		**125**	**500**	**500**	**520**	**520**	**520**